


실란과 PCPA 그래프팅의 동시적인 영향이 BN 및 GO 하이브리드 복합체의 열 및 기계적 특성에 미치는 영향

조영성*[#] · 김지훈*[#] · 조장우* · 김주현*^{*,**†} 

*중앙대학교 화학공학과

**중앙대학교 대학원 지능형에너지산업학과

(2024년 4월 29일 접수, 2024년 5월 23일 수정, 2024년 5월 28일 채택)

Impact of Simultaneous Silane and PCPA Grafting on the Thermal and Mechanical Properties of BN and GO Hybrid Composites

Youngsung Cho*[#], Jihoon Kim*[#], Jangwoo Cho*, and Jooheon Kim*^{*,**†} 

*Department of Chemical Engineering, Chung-Ang University, 84 Heukseok-ro, Dongjak-gu, Seoul 06974, Korea

**Department of Intelligent Energy and Industry, Graduate School, Chung-Ang University, Seoul 06974, Korea

(Received April 29, 2024; Revised May 23, 2024; Accepted May 28, 2024)

초록: 본 연구에서는 붕화붕소(BN) 및 그래핀 산화물(GO) 하이브리드 필러를 사용하여 고열전도성 복합체를 개발하였다. 폴리(카테콜/폴리아민)(PCPA) 및 실란 필러를 동시 그래프팅하는 절차를 채택하여 에폭시 중합체의 열 및 기계적 특성을 향상시켰다. (3-글리시디록시프로필)트리메톡시실란(GPTMS), 폴리카테콜 및 테트라에틸렌펜타민을 사용한 표면 처리는 수지 매트릭스 내 필러 응집을 최소화했다. 결과물로 나온 표면 처리된 하이브리드 복합체는 기본 매트릭스와 비교하여 열 전도도가 놀라운 2252% 증가한 것으로 나타났다(4.83 Wm⁻¹K⁻¹). 이 향상은 50 wt% 표면 처리된 BN, 5 wt% 표면 처리된 GO, 그리고 PCPA 및 GPTMS 처리를 포함하여 구현되었다. 반면, 날 것의 필러를 함유하는 복합체는 열 전도도가 낮았다(3.37 Wm⁻¹K⁻¹). 표면 처리된 필러 함유 복합체는 또한 우수한 기계적 특성을 나타냈다. 이러한 표면 처리의 장점과 PCPA 및 GPTMS를 이용한 간편한 열 가공 절차는 전자 패키지 재료의 열 분산 문제에 대한 편리하고 신속한 해결책을 제공한다.

Abstract: In this study, we developed highly thermally conductive composites using boron nitride (BN) and graphene oxide (GO) hybrid fillers. By employing a simultaneous grafting procedure involving poly(catechol/polyamine) (PCPA) and silane fillers, we enhanced the thermal and mechanical properties of an epoxy polymer. Surface treatments with (3-glycidyloxypropyl)trimethoxysilane (GPTMS), polycatechol, and tetraethylenepentamine minimized filler aggregation within the resin matrix. The resulting surface-treated hybrid composite exhibited a remarkable 2252% increase in thermal conductivity (4.83 Wm⁻¹K⁻¹) compared to the base matrix. This improvement was achieved by incorporating 50 wt% surface-treated BN, 5 wt% surface-treated GO, and PCPA and GPTMS treatments. In contrast, composites containing raw fillers demonstrated lower thermal conductivity (3.37 Wm⁻¹K⁻¹). The surface-treated filler-contained composites also showed superior mechanical properties. The advantages of this surface treatment, combined with the straightforward thermal curing procedure involving PCPA and GPTMS, offer a convenient and rapid solution for heat dissipation challenges in electronic packaging materials.

Keywords: thermal conductivity, mechanical property, surface treatment.

Introduction

The demand for high-power, portable, and miniaturized devices has increased owing to rapid advancements in the fields of

technologies such as automobiles,¹⁻³ packaging materials, and integrated electronic components (e.g., printed circuit boards and micro light-emitting diodes).⁴⁻⁷ However, these technological advancements have issues, such as heat accumulation, which causes device malfunction and degradation. To address these issues, thermal interface materials (TIMs) have emerged as crucial tools for enhancing heat dissipation and electrical insulation.⁸⁻¹⁰ Among all TIMs, polymer composites play an indis-

[#]These authors contributed equally to this work.

[†]To whom correspondence should be addressed.

jooheonkim@cau.ac.kr, [ORCID](https://orcid.org/0000-0002-6644-7791) 0000-0002-6644-7791

©2024 The Polymer Society of Korea. All rights reserved.

pensable role in electronic devices because of their low cost, ease of processing, lightweight properties, flexibility, and electrical insulating properties.^{11–13} Nevertheless, their inherent low thermal conductivity ($<0.4 \text{ Wm}^{-1}\text{K}^{-1}$) remains a major concern.^{14,15} To overcome this limitation, various thermally conductive fillers, including graphene,^{16,17} graphene oxide (GO),^{18,19} carbon nanotubes,²⁰ MXenes,^{21,22} boron nitride (BN),²³ and aluminum nitride,²⁴ have been used to enhance the thermal properties of polymers.

Hexagonal BN is one of the most commonly employed ceramic fillers for producing high-thermal-conductivity composites.²⁵ Its popularity stems from its inherent attributes, including high in-plane thermal conductivities of $185\text{--}300 \text{ Wm}^{-1}\text{K}^{-1}$, exceptional chemical stability, improved insulating characteristics, and low dielectric properties.²⁶ These attributes are particularly essential in applications involving electronic devices.

Graphene has recently attracted significant attention in research because of its remarkably high thermal conductivity of $\sim 5300 \text{ Wm}^{-1}\text{K}^{-1}$,²⁷ which is achieved through two-dimensional phononic and electronic transport pathways.²⁸ Generally, there are two crucial factors for achieving the desired thermal conductivity in polymer composites: ensuring the uniform dispersion of fillers within the matrix and promoting strong interfacial adhesion.²⁹ Unfortunately, although graphene exhibits impressive performance as a filler, the strong interactions among its sp^2 -conjugated carbon sheets can lead to aggregation within the polymer matrix. Additionally, the limited compatibility between graphene and the matrix results in poor interfacial interactions, creating acoustic phonon mismatches. These mismatches hinder heat transfer within the composite by introducing thermal boundary resistance. To overcome these limitations, various approaches, including the chemisorption or physisorption of organic compounds using grafting or coating techniques, have been explored to functionalize the surface of graphene.^{30,31}

Silane coupling agents have been utilized to establish robust connections between organic and inorganic materials.^{32,33} These agents typically consist of silicon atoms, hydrolyzable com-

ponents, linkers (usually alkyl linkers), and an organofunctional group. In our experiment, (3-glycidyloxypropyl)trimethoxysilane (GPTMS) was chosen as the silane coupling agent because of the presence of its epoxide group within the epoxy resin backbone.

The widespread use of dopamine in industrial applications is limited by its high cost.³⁴ Nevertheless, catechol structures and amino-terminal groups exhibit structural similarity to dopamine, offering them the potential for promoting strong adhesion. Therefore, in this study, catechol and polyamine were used as a cost-effective alternative to poly(dopamine) to synthesize poly(catechol/polyamine) (PCPA).

In this study, composites were developed using bisphenol A diglycidyl ether (DGEBA) and surface-treated BN and GO fillers. Generally, the silane treatment of such fillers is known to be a challenging process. Therefore, the use of PCPA is a low-cost and straightforward method that allows for the attachment of GPTMS to the filler surface through polymerization at a suitable pH. This innovative method of creating polymer composites with high thermal conductivity ushers in a new chapter in electronic packaging materials because of its simplicity and low cost.

Experimental

Materials. GO powder was sourced from Grapheneall Co., Republic of Korea. Hexagonal BN powder (purity level: 99% and average diameter: $12 \mu\text{m}$) was provided by Momentive Performance Materials Inc., USA. DGEBA was supplied by Kukdo Chemical Co., Republic of Korea. Jeffamine D-230 (DDM) curing agent was supplied by New Seoul Chemical Co., Korea. GPTMS, polycatechol, and tetraethylenepentamine (TEPA) were obtained from Sigma-Aldrich. Ethanol, distilled water, acetic acid, and hydroiodic acid were supplied by Daejung Chemical Co., Republic of Korea.

Preparation of Surface-treated BN. Figure 1 demonstrates surface treatment of fillers. BN was hydroxylated before the

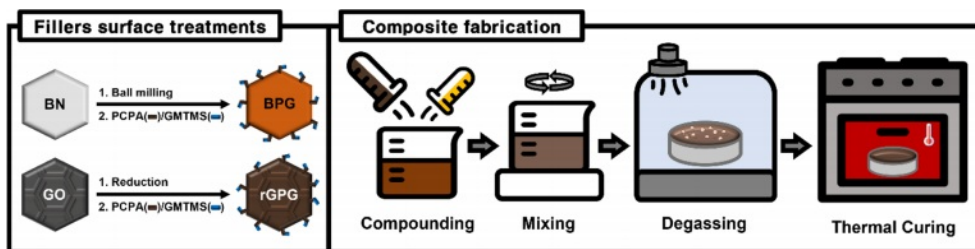


Figure 1. Schematic of the surface treatment and composite fabrication processes.

silane and PCPA molecules were attached to its surface. BN hydroxylation process involved ball milling it with zirconia balls at 500 rpm. First, the BN powder was dispersed in distilled water in a 500 mL plastic bottle. The zirconia balls were subsequently added to the bottle, and ball milling was conducted for 48 h. The filtered hydroxylated BN cakes were then dried in a vacuum oven at 50 °C for 48 h to remove any residual solvent. Catechol and TEPA were dissolved in 200 mL of water to obtain a solution pH of 9.5 and a molar ratio of 3:1. Catechol and PETA were dissolved in 200 mL of water. Afterward, the dried hydroxylated BN was redispersed in the water. GPTMS was combined with the hydroxylated BN solution in a weight ratio of 1:10. This solution was mixed on a hotplate at 60 °C and 500 rpm for 4 h. Subsequently, the solution was filtered and dried in a vacuum oven at 70 °C for 48 h. The resulting material, which was treated with catechol, TEPA, and GPTMS, was designated as BPG.

Preparation of Surface-treated GO. GO was subjected to a reduction process using a reduction solution that comprised hydroiodic acid and acetic acid in a 3:1 volume ratio. Initially, 5 g of GO was dispersed in 200 mL of the reduction solution, which was then stirred with a magnetic bar at 500 rpm for 24 h to produce reduced GO (rGO). Subsequently, the acidic rGO mixture was filtered with distilled water three times to neutralize its pH. The rGO cakes obtained from the filtration process were then dried in the vacuum oven at 70 °C for 48 h.

Catechol and TEPA were combined in a molar ratio of 3:1 to produce PCPA, while GPTMS and rGO were combined in a weight ratio of 1:10 for the silane treatment. The catechol, TEPA, rGO, and GPTMS were mixed with 200 mL of distilled water. The solution was then stirred in an oil bath at 60 °C and 500 rpm for 4 h. The resulting material, which was subjected to PCPA and silane treatment, was subsequently filtered and dried in the vacuum oven at 70 °C for 48 h. This PCPA and

silane-treated rGO product was labeled as rGPS.

Fabrication of the Composites. Figure 1 depicts the composite fabrication process. The fillers, namely, DGEBA, BPG, and rGPS, were mixed with epoxy in a planetary paste mixer for 10 min and degassed for 5 min in a designated ratio. Thereafter, the thermal curing agent, DDM, was added to the mixture, which was subsequently mixed for 5 min. The resulting mixture was then placed in TEFLON and silicon molds to yield the final composites. To mitigate the formation of voids due to air pockets, the sample mixtures were placed in the vacuum oven at 30 °C for 3 h. Next, the samples were placed in an oven at 150 °C for 30 min. The fabricated composites were designated based on the type and composition of fillers used. Table 1 presents the composition and corresponding designations of the composites.

Characterization. The morphological characteristics of the matrices, fillers, and composites were evaluated using field-emission scanning electron microscopy (FE-SEM; Sigma, Carl Zeiss). The functional attributes of the matrices and the surface modifications of the fillers were evaluated using Fourier-transform infrared (FTIR) spectroscopy (Spectrum One, PerkinElmer, USA) in the attenuated total reflection mode at wavelengths ranging from 4000 to 400 cm^{-1} . X-ray photoelectron spectroscopy (XPS) was conducted using an ESCA 2000 X-ray photoelectron spectrometer (VG Microtech) to scrutinize the surface properties of the BN and GO fillers. The crystalline nature of both the matrices and fillers was confirmed via X-ray diffraction (XRD; New D8-Advance, Bruker-AXS) within a 2θ range of 10°–80°. The thermal stability and degradation properties of the matrices, fillers, and composites were assessed using thermogravimetric analysis (TGA; TGA 2050, TA Instruments) at temperatures of 50–800 °C in a nitrogen atmosphere. The tensile strength and tensile strain of the matrices and composites were determined using a universal testing machine (3344Q9465,

Table 1. Compositions of the Matrices and Composites

Composite	Matrix		Filler			Total
	DGEBA	BN	BPG	GO	rGPG	
BN50	50.0%	50.0%	–	–	–	100.0
BP10	90.0%	–	10.0%	–	–	100.0
BP30	70.0%	–	30.0%	–	–	100.0
BP50	50.0%	–	50.0%	–	–	100.0
BN50/GO5	45.0%	50.0%	–	5.0%	–	100.0
BP50/GP1	49.0%	–	50.0%	–	1.0%	100.0
BP50/GP3	47.0%	–	50.0%	–	3.0%	100.0
BP50/GP5	45.0%	–	50.0%	–	5.0%	100.0

Instron Co., Norwood, MA, USA) at a crosshead speed of 10 mm min⁻¹. Additionally, the storage modulus, loss modulus, and tan delta were measured via dynamic mechanical analysis (DMA; PerkinElmer DMA 8000, PerkinElmer, Waltham, MA, USA) at temperatures ranging from 30 °C to 150 °C, a heating rate of 3 °C/min, and a frequency of 1 Hz.

The thermal conductivity was calculated using Eq. (2) with the measured values:

$$K = \alpha \cdot \rho \cdot C_p \quad (2)$$

where K represents the thermal conductivity, ρ is the density, α is the thermal diffusivity, and C_p is the heat capacity of the composite.

The thermal diffusivity, specific heat capacity, and bulk density were measured using laser flash analysis (LFA) (NanoFlash LFA 467, Netzsch Instruments Co., Selb, Germany), differential scanning calorimetry (DSC-7, PerkinElmer Co.), and an electromagnetic balance (HR-250AZ, A&D Company Limited, Tokyo, Japan) based on the Archimedes principle.

Finally, the thermal conductivity enhancement (TCE) was calculated using Eq. (3):

$$\text{TCE} = \frac{K - K_m}{K_m} \times 100\% \quad (3)$$

where K_m represents the thermal conductivity of the matrix.

Results and Discussion

Filler Characterization. Figure 2 shows a comparison of the morphological characteristics of the BN and GO fillers, tak-

ing into account whether or not they underwent surface treatment. In Figure 2(b), BN was subjected to hydroxylation through ball-milling with zirconia balls, resulting in a fractured and thinner BN surface, which signifies the successful production of BN nanosheets (BNNS) via the ball-milling and hydroxylation processes. As shown in Figure 2(d), the BNNS surfaces were modified by PCPA and GPTMS. Notably, the raw BN molecules were clean and orderly, but BPG had smoothly grafted molecules. However, the surface of BPG was uneven, indicating the presence of PCPA and GPTMS. Contrarily, rGO had a smooth surface after GO reduction, but the grafted surface-treatment agents remained visible on its surface after the grafting procedure. These effective surface modifications were demonstrated by the morphological changes observed through FE-SEM analysis.

The FTIR and XPS spectra are presented in Figure 3 to compare the chemical properties of the BN and GO fillers in various states. Figure 3(a) shows the FTIR spectra of raw BN and hydroxylated BN grafted with PCPA and GPTMS (BPG). Notably, the FTIR spectra of both BN and BPG exhibit B–N absorption peaks at about 760 and 1300 cm⁻¹.³⁵ However, the FT-IR spectrum of BPG displays peaks at 1130, 1272, and 3392 cm⁻¹, which correspond to two Si–O–Si and one O–H absorption peak, respectively.³⁶

Figure 3(b) depicts the FTIR spectra of raw GO, rGO, and rGPG. The FTIR spectrum of rGO exhibits peaks at 1341, 1642, 2919, and 3397 cm⁻¹, which are attributed to C–C stretching, C=O stretching, C–H stretching, and O–H stretching respectively,³⁷ indicating that the reduction process was successful. Further-

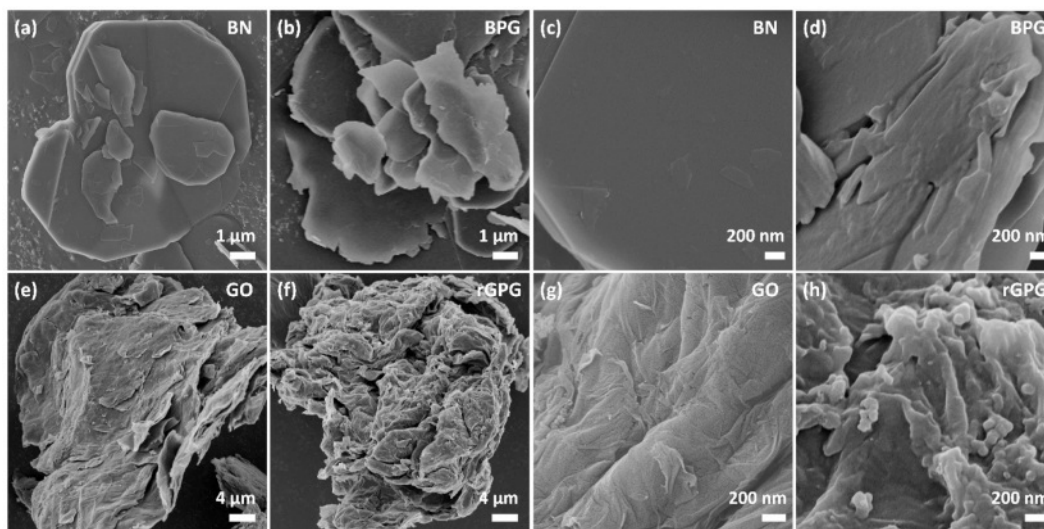


Figure 2. FE-SEM images of (a) BN in low magnification; (b) BPG in low magnification; (c) BN in high magnification; (d) BPG in high magnification. (e) GO in low magnification; (f) rGPG in low magnification; (g) GO in high magnification; (h) rGPG in high magnification.

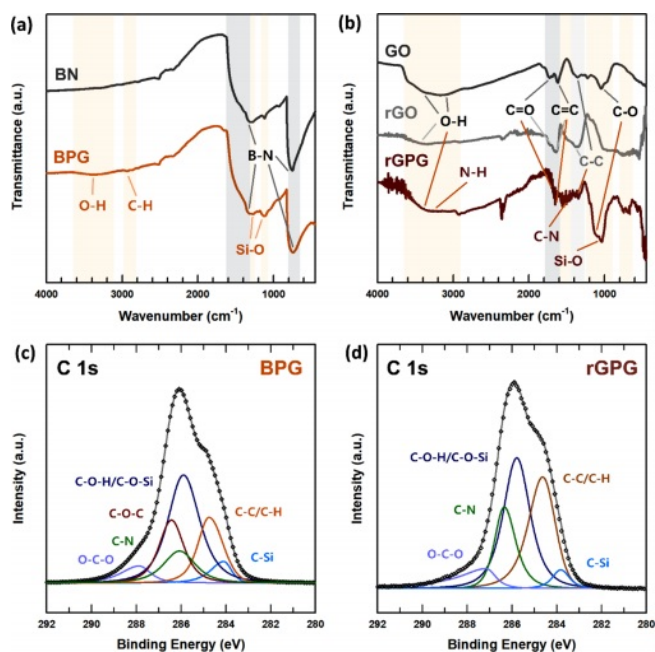


Figure 3. FTIR spectra of (a) BN, BPG; (b) GO, rGO, and rGPG. XPS C 1s deconvolution spectra of (c) BPG; (d) rGPG.

more, the FT-IR spectrum of rGPG exhibits distinctive peaks at 1040, 1583, 1657, 1701, 2934, 3170, and 3347 cm^{-1} , which

correspond to Si-O stretching, C-O stretching, C-N stretching, C=C stretching, C=O stretching, N-H stretching, and O-H, respectively.³⁸ These peaks observed in the rGO and rGPG spectra confirm the successful reduction and surface treatment of GO.

XPS analysis was conducted to further validate the presence of PCPA and GPTMS on the surfaces of the GO and BN fillers. Figures 3(c) and 3(d) show the C 1s deconvolution spectra of BPG and rGPG, respectively. BPG exhibits deconvoluted C 1s peaks corresponding to C-Si (284.0 eV), C-C/C-H (284.8 eV), and C-O-H/C-O-Si (285.9 eV), C-N (286.1 eV), C-O-C (286.5 eV), and O-C-O (287.9 eV) bonds. Similarly, rGPG exhibits peaks corresponding to C-Si (283.8 eV), C-C/C-H (284.6 eV), C-O-H/C-O-Si (285.8 eV), C-N (286.3 eV) and O-C-O (287.2 eV) bonds.³⁹ The polymerization of PCPA and the presence of grafted silane molecules can be observed in the XPS deconvolution spectra. It is worth noting that there was a slight shift in the binding energy due to the different surface treatments. In summary, both the FTIR and XPS spectra confirm that the surface treatment of the fillers was successful.

The thermal degradation properties of the fillers were examined to evaluate their thermal stability and the composition of the surface-treatment agents, as shown in Figures 4(a-c). The

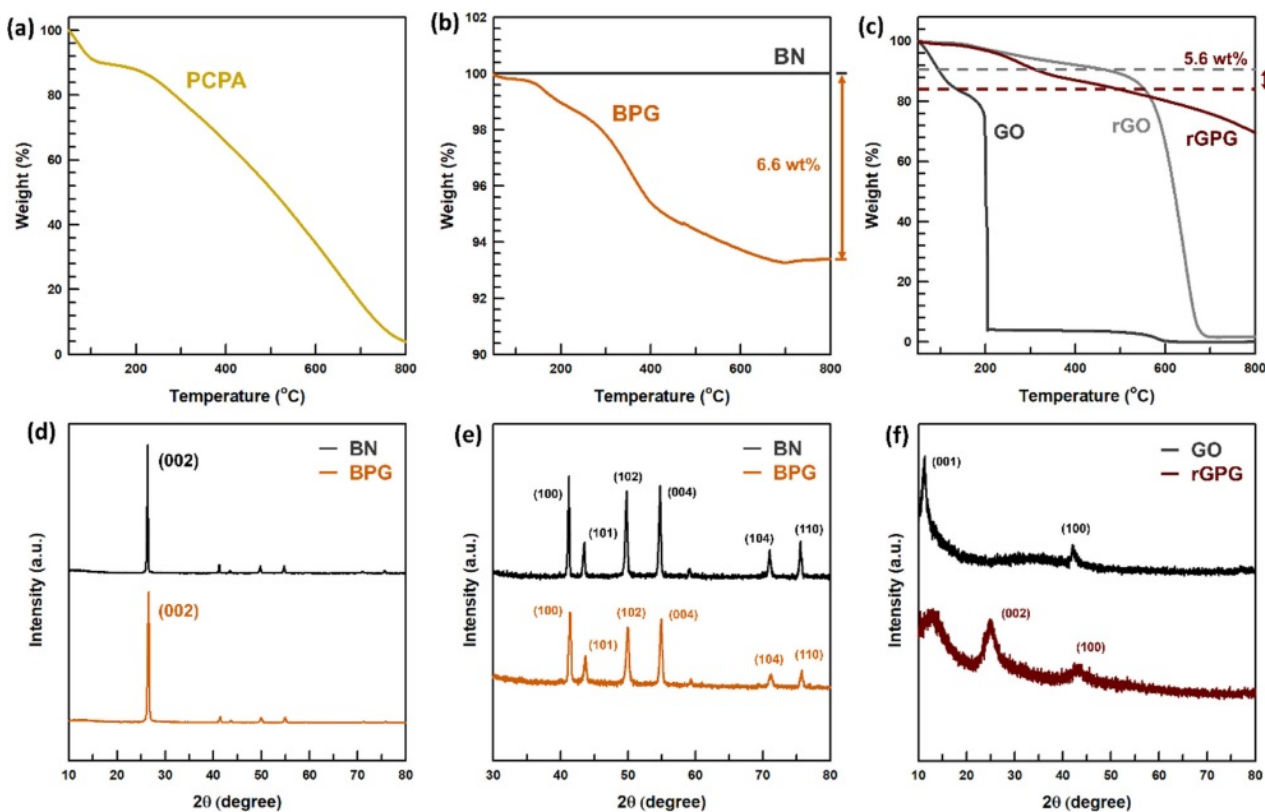


Figure 4. TGA curves of (a) PCPA; (b) BN and BPG; (c) GO, rGO, and rGPG. XRD spectra of (d,e) BN and BPG; (f) GO and rGPG.

thermal stability of PCPA was examined as a reference. The results revealed that the weight gradually decreased as the temperature increased. Raw BN displayed high thermal stability, with a degradation temperature of 2973 °C.⁴⁰ According to the TGA curves of BPG, the weight gradually decreased as the temperature increased, indicating the successful grafting of the PCPA and silane molecules. When raw GO, rGO, and rGPG were compared, it was discovered that raw GO demonstrated a thermally stable profile until ~200 °C, rGO started to degrade at about 625 °C, and rGPG displayed a thermally stable profile. The reduction of GO and the polymerization of PCPA with GPTMS on the GO surface enhanced the thermal stability. Based on the TGA curves, the compositions of the surface-treatment agents in BPG and rGPG were calculated to be 6.6% and 5.6%, respectively.

The TGA curves and XRD spectra of the fillers are compared in Figure 4 to assess their properties. The XRD spectrum of BPG exhibits distinctive patterns with peaks near 26.64°, 41.41°, 43.63°, 50.02°, 54.94°, 71.21°, and 75.78°, which cor-

respond to the (002), (100), (101), (102), (004), (104), and (110) planes, respectively.⁴¹ Notably, the XRD pattern of BPG is similar to that of raw BN, but it is slightly shifted to the right. The XRD patterns of GO display peaks at 11.39° and 42.10°, which correspond to the (001) and (100) planes, respectively. Conversely, the XRD patterns of rGPG display distinct peaks at 42.27°, 42.76°, and 42.86°, which can be attributed to the reduction of GO.⁴² The XRD pattern of each filler exhibits minor shifts, suggesting that the hydroxylation process and the attachment of the surface-treatment agents had a modest impact on the crystallinity of the fillers.⁴³

Composite Characterization. Figure 5 displays cross-sectional FE-SEM images of the composites. To ensure a smooth surface for analysis, the samples were cryogenically frozen with liquid nitrogen and then fractured before FE-SEM imaging. The filler surfaces in the raw filler-containing composites appeared clean and neat. Moreover, BN and GO were distinct and separate in these raw filler-containing composites. Addi-

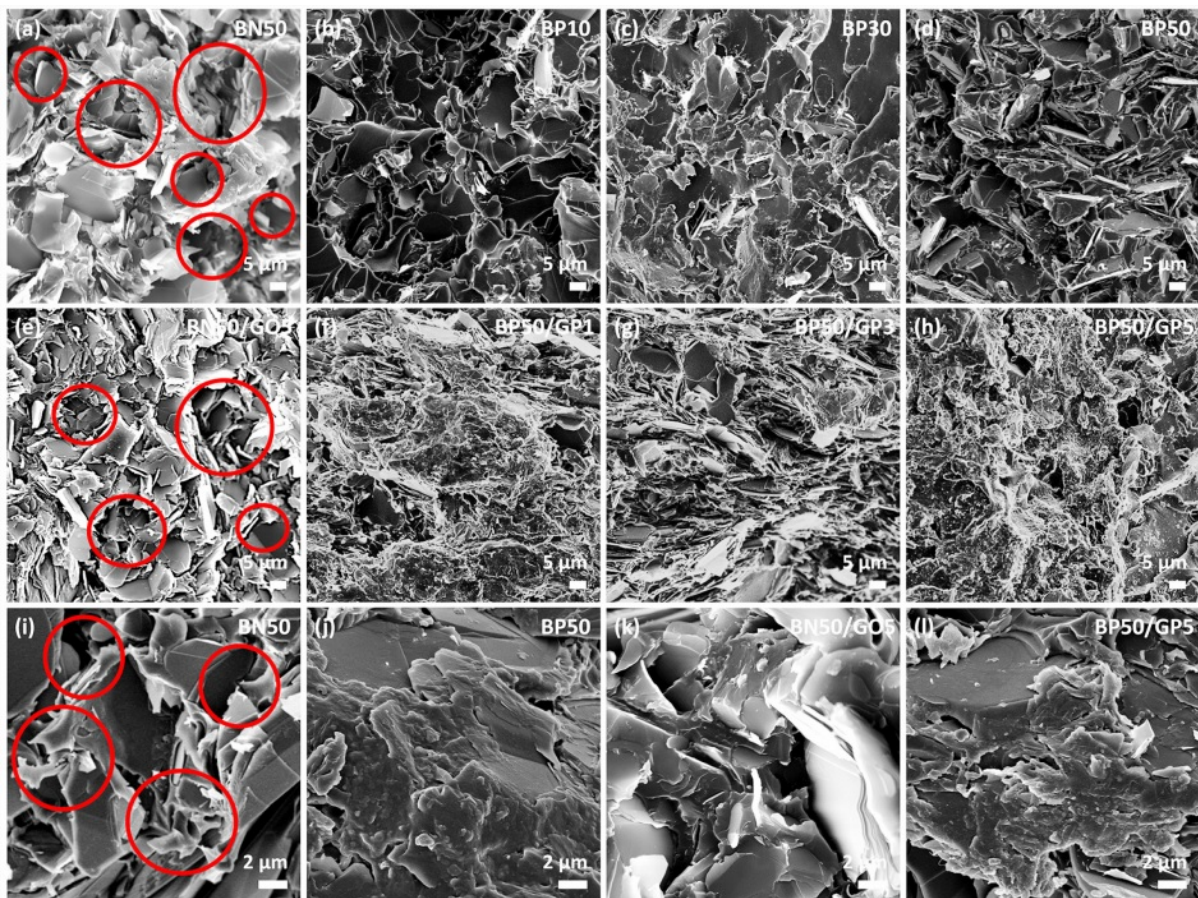


Figure 5. Cross-sectional FE-SEM images of (a) BN50; (b) BP10; (c) BP30; (d) BP50; (e) BN50/GO5; (f) BP50/GP1; (g) BP50/GP3; (h) BP50/GO3 in low magnification. Cross-sectional FE-SEM images of (i) BN50; (j) BP50; (k) BN50/GO5; (l) BP50/GP5 in high magnification. (The red circles indicate voids.)

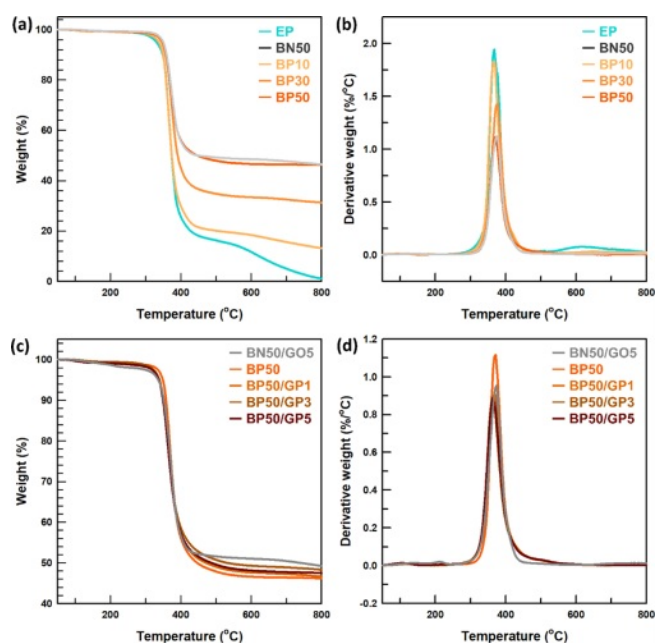


Figure 6. (a, b) TGA curves; (c, d) dTG curves of the composites.

tionally, the BN50 and BN50/GP5 raw filler-containing composites had substantial voids due to the aggregation of the BN and GO fillers. By performing simultaneous PCPA and GPTMS surface treatments, the miscibility of the BN fillers improved. This is because the surface-treatment agents acted as a bridge between the matrix and BN, effectively filling the voids. In contrast, both the surface-treated BN and GO fillers in the surface-treated composites adhered successfully to the matrix owing to the surface treatment. Consequently, the surface-treated composites were expected to have relatively high thermal conductivities.

As illustrated in Figure 6, we performed TGA and dTG analyses on the composites. The composites were found to exhibit higher thermal stability than the matrix, which exhibited the highest weight loss, as depicted in Figure 6. Since PCPA exhibited a gradual weight loss as the temperature increased, the surface-treated composites also exhibited a slight and gradual weight loss before and after 400 °C. The incorporation of the BN and GO fillers into the matrix significantly enhanced the thermal stability of the resin. A similar pattern was observed in the dTG analysis. A similar trend was observed in the dTG analysis results, further confirming that the surface treatment and filler addition were successful.

Figures 7(a-b) show a comparison of the mechanical properties of the composites. The composites were found to exhibit a gradual decrease of mechanical strength upon filler addition.

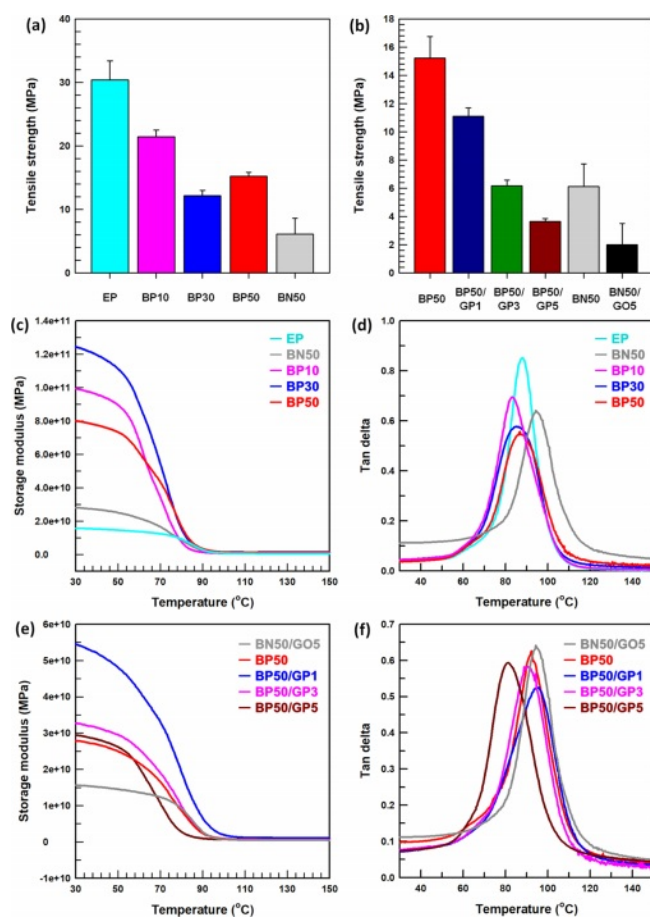


Figure 7. (a) Tensile strength; (b) elongation at break of the composites; (c, e) storage modulus; (d, f) tan delta of the composites.

However, the surface-treated composites exhibited higher tensile strength than the raw filler-containing composites. Specifically, BP50 and BN50 exhibited tensile strength values of 15.4 MPa and 5.3 MPa, respectively. The hybrid filler composites exhibited a similar trend, with BP50/GP5 exhibiting a tensile strength of 3.65 MPa and BN50/GO5 exhibiting 3.29 MPa. The composites exhibited similar elongation at break values. Overall, the surface-treatment agents not only improved the dispersibility of the fillers in the matrix but also significantly enhanced the mechanical properties.

Figures 7(c-f) provide a comparison of the storage modulus and tan delta. Storage modulus and tan delta showed trends of general increase with the incorporation of BPG filler, but decrease with the incorporation of rGPG filler. As observed in UTM results, DMA results confirm that the inclusion of various fillers decreases mechanical properties.

Figures 8(a-d) present a comparison of the thermal conductivities and TCEs of the matrix and composites. The thermal

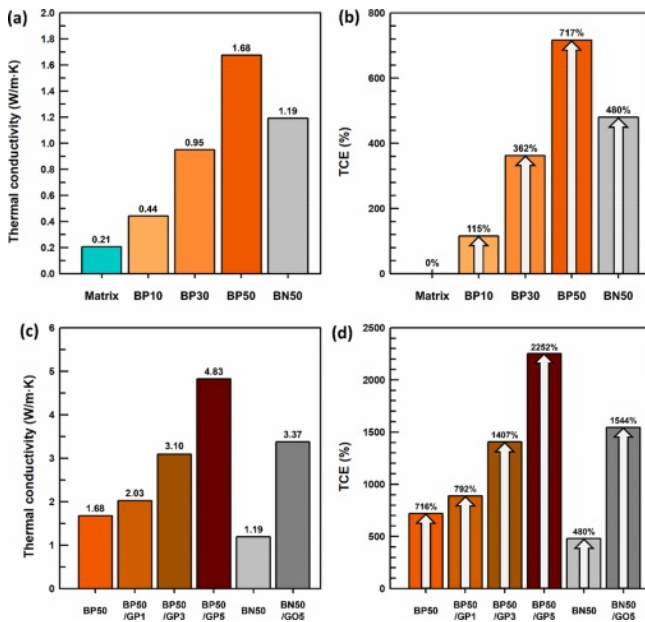


Figure 8. (a) Thermal conductivities; (b) thermal conductivity enhancements of the matrix, BP, and BN composites; (c) thermal conductivities; (d) thermal conductivity enhancements of the BP, BP/GP, BN, and BN/GO composites.

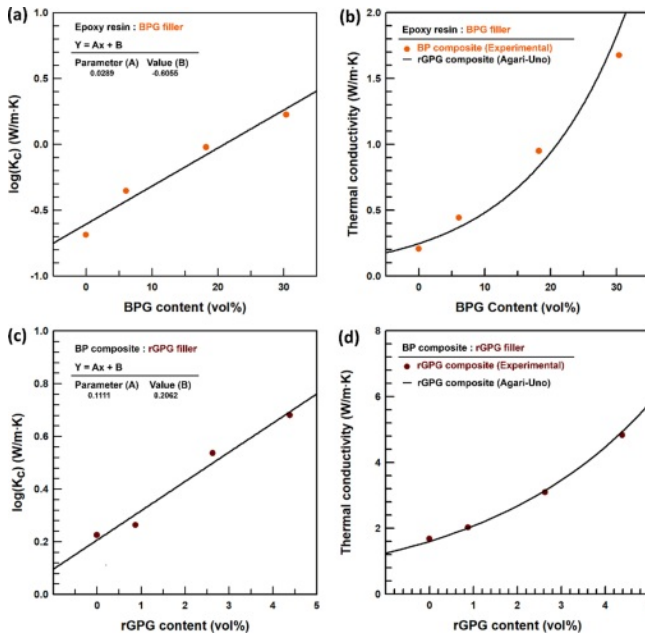


Figure 9. Agari-uno modeling of the (a-b) BP composites; (c-d) BP/GP composites.

conductivities of the matrix and the composites, namely, EP, BP10, BP30, BP50, BN50, BP50/GP1, BP50/GP3, BP50/GP5, and BN50/GO5, were measured to be 0.21, 0.44, 0.95, 1.68, 1.19, 2.03, 3.10, 4.83, and 3.37 $\text{Wm}^{-1}\text{K}^{-1}$, respectively. Notably, BP50/GP5 demonstrated the most significant enhancement, with a

remarkable 2252% increase in thermal conductivity. Surface treatment on the hybrid fillers was successful in increasing the thermal conductivity of the composites. The incorporation of GO and BN hybrid filler with surface treatment showed the highest TCE among the composites.

In Figure 9, the thermal conductivity of the composites was analyzed based on the agari-uno model.⁴⁴ The theoretical and experimental values were compared. Figure 9(a-b) and Figure 9(c-d) were analyzed based on the BPG content compared to epoxy resin and rGPG filler content to BP50 composites in volume percentage, respectively. The agari-uno model shows that the experimental thermal conductivities fit well. The further discussion of the Agari-uno model is discussed in the supplementary information.

Conclusions

In this study, we developed epoxy-based composites with high thermal conductivity by employing a hybrid filler composite comprising BN and GO. We focused on investigating the effect of a simultaneous grafting procedure involving PCPA and silane surface-treatment agents on the thermal and mechanical properties of epoxy polymers. To overcome the challenges related to the aggregation of fillers within the resin matrix, we employed surface-treatment agents, namely, GPTMS, catechol, and TEPA. PCPA was polymerized on the filler surfaces, effectively bridging the fillers and matrix. The resulting surface-treated hybrid composite exhibited a high thermal conductivity of $4.83 \text{ Wm}^{-1}\text{K}^{-1}$, which is a 2252% increase compared to the matrix. This enhancement was achieved by employing 50 wt% surface-treated BN, 5 wt% surface-treated GO, and PCPA and GPTMS treatments. In contrast, the composite containing 50 wt% raw BN and 5 wt% raw GO fillers exhibited a thermal conductivity of $3.37 \text{ Wm}^{-1}\text{K}^{-1}$. This demonstrates that the surface-treated filler composites exhibited significantly higher thermal conductivity and better mechanical properties than the raw filler-containing composites. The advantages of surface treatment, along with the straightforward thermal curing procedure involving PCPA and GPTMS, offer a convenient and rapid solution for addressing the heat dissipation issues in electronic packaging materials.

Acknowledgments: This research was supported by the Chung-Ang University research grant in 2022 and supported by the MSIT (Ministry of Science and ICT), Korea, under the ITRC (Information Technology Research Center) support pro-

gram (IITP-2023-2020-0-01655) supervised by the IITP.

Conflict of Interest: The authors declare that there is no conflict of interest.

Supporting Information: Information is available regarding the density, heat capacity, thermal diffusivity, and thermal conductivity. Also, the detailed procedure of the modeling is available. The materials are available *via* the Internet at <http://journal.polymer-korea.or.kr>.

References

- Liu, B.; Yang, J.; Zhang, X.; Yang, Q.; Zhang, J.; Li, X. Development and Application of Magnesium Alloy Parts for Automotive OEMs: A Review. *J. Magnes. Alloy.* **2023**, *11*, 15-47.
- Pan, Y.; Stark, R. An Interpretable Machine Learning Approach for Engineering Change Management Decision Support in Automotive Industry. *Comput. Ind.* **2022**, *138*, 103633-103650.
- Savari, G F.; Sathik, M. J.; Raman, L. A.; El-Shahat, A.; Hasanien, H. M.; Almakhles, D.; Abdel Aleem, S. H. E.; Omar, A. I. Assessment of Charging Technologies, Infrastructure and Charging Station Recommendation Schemes of Electric Vehicles: A Review. *Ain. Shams. Eng. J.* **2023**, *14*, 101938-101952.
- Sun, Z.; Li, J.; Yu, M.; Kathaperumal, M.; Wong, C. P. A Review of the Thermal Conductivity of Silver-Epoxy Nanocomposites as Encapsulation Material for Packaging Applications. *Chem. Eng. J.* **2022**, *446*, 137319-137332.
- Li, R.; Yang, X.; Li, J.; Shen, Y.; Zhang, L.; Lu, R.; Wang, C.; Zheng, X.; Chen, H.; Zhang, T. Review on Polymer Composites with High Thermal Conductivity and Low Dielectric Properties for Electronic Packaging. *Mater. Today. Phys.* **2022**, *22*, 100594-100611.
- Wen, Y.; Chen, C.; Ye, Y.; Xue, Z.; Liu, H.; Zhou, X.; Zhang, Y.; Li, D.; Xie, X.; Mai, Y. W. Advances on Thermally Conductive Epoxy-Based Composites as Electronic Packaging Underfill Materials—A Review. *Adv. Mater.* **2022**, *34*, 2201023-2201044.
- Park, D.; Ju, H.; Kim, J. Enhanced Thermoelectric Properties of Flexible N-Type Ag₂Se Nanowire/Polyvinylidene Fluoride Composite Films Synthesized via Solution Mixing. *J. Ind. Eng. Chem.* **2021**, *93*, 333-338.
- An, D.; He, R.; Chen, J.; Li, Z.; Sun, Z.; Yu, H.; Liu, Y.; Zhang, Z.; Feng, W.; Wong, C. Interacted Boron Nitride/Mxene Hybrids with Vertically Aligned Networks for Improving the Thermal Conductivity, Electromagnetic Wave Absorption and Mechanical Properties for the Polymer-Based Thermal Interface Materials. *Compos. Part. A. Appl. Sci. Manuf.* **2023**, *174*, 107727-107735.
- Hu, Q.; Bai, X.; Zhang, C.; Zeng, X.; Huang, Z.; Li, J.; Li, J.; Zhang, Y. Oriented BN/Silicone Rubber Composite Thermal Interface Materials with High out-of-Plane Thermal Conductivity and Flexibility. *Compos. Part. A. Appl. Sci. Manuf.* **2022**, *152*, 106681-106688.
- Xie, Z.; Dou, Z.; Wu, D.; Zeng, X.; Feng, Y.; Tian, Y.; Fu, Q.; Wu, K. Joint-Inspired Liquid and Thermal Conductive Interface for Designing Thermal Interface Materials with High Solid Filling yet Excellent Thixotropy. *Adv. Funct. Mater.* **2023**, *33*, 2214071-2214079.
- Wu, Q.; Li, W.; Liu, C.; Xu, Y.; Li, G.; Zhang, H.; Huang, J.; Miao, J. Carbon Fiber Reinforced Elastomeric Thermal Interface Materials for Spacecraft. *Carbon* **2022**, *187*, 432-438.
- Chung, D. D. L. A Critical Review of Carbon-Based Thermal Interface Materials. *Mater. Chem. Phys.* **2023**, *309*, 128432-128440.
- An, D.; Chen, Y.; He, R.; Yu, H.; Sun, Z.; Liu, Y.; Liu, Y.; Lian, Q.; Feng, W.; Wong, C. The Polymer-Based Thermal Interface Materials with Improved Thermal Conductivity, Compression Resilience, and Electromagnetic Interference Shielding Performance by Introducing Uniformly Melamine Foam. *Adv. Compos. Hybrid. Mater.* **2023**, *6*, 136-146.
- Zhao, H. Y.; Yu, M. Y.; Liu, J.; Li, X.; Min, P.; Yu, Z. Z. Efficient Preconstruction of Three-Dimensional Graphene Networks for Thermally Conductive Polymer Composites. *Nano-Micro. Lett.* **2022**, *14*, 129-168.
- Yu, H.; Chen, C.; Sun, J.; Zhang, H.; Feng, Y.; Qin, M.; Feng, W. Highly Thermally Conductive Polymer/Graphene Composites with Rapid Room-Temperature Self-Healing Capacity. *Nano-Micro. Lett.* **2022**, *14*, 135-148.
- Lin, H.; Jian, Q.; Bai, X.; Li, D.; Huang, Z.; Huang, W.; Feng, S.; Cheng, Z. Recent Advances in Thermal Conductivity and Thermal Applications of Graphene and Its Derivatives Nanofluids. *Appl. Therm. Eng.* **2023**, *218*, 119176-119202.
- Tan, X.; Yuan, Q.; Qiu, M.; Yu, J.; Jiang, N.; Lin, C. Te; Dai, W. Rational Design of Graphene/Polymer Composites with Excellent Electromagnetic Interference Shielding Effectiveness and High Thermal Conductivity: A Mini Review. *J. Mater. Sci. Technol.* **2022**, *117*, 238-250.
- Chen, Q.; Liu, L.; Zhang, A.; Wang, W.; Wang, Z.; Zhang, J.; Feng, J.; Huo, S.; Zeng, X.; Song, P. An Iron Phenylphosphinate @graphene Oxide Nanohybrid Enabled Flame-Retardant, Mechanically Reinforced, and Thermally Conductive Epoxy Nanocomposites. *Chem. Eng. J.* **2023**, *454*, 140424.
- Li, Y.; Zhang, T.; Zhang, Y.; Zhao, C.; Zheng, N.; Yu, W. A Comprehensive Experimental Study Regarding Size Dependence on Thermal Conductivity of Graphene Oxide Nanosheet. *Int. Commun. Heat Mass Transf.* **2022**, *130*, 105764.
- Cho, Y.; Han, S.; Kim, J. Improved Thermal, Dielectric, and Mechanical Properties of Acrylate Composites with Diethylene Glycol and Silane-Treated Ternary Hybrid Fillers via Three-Dimensional Vat Photopolymerization. *Mater. Chem. Phys.* **2023**, *309*, 128360.
- Li, M.; Sun, Y.; Feng, D.; Ruan, K.; Liu, X.; Gu, J. Thermally Conductive Polyvinyl Alcohol Composite Films via Introducing Hetero-Structured MXene@silver Fillers. *Nano. Res.* **2023**, *16*, 7820-7828.
- Li, Y.; Zhang, D.; Zhou, B.; He, C.; Wang, B.; Feng, Y.; Liu, C. Synergistically Enhancing Electromagnetic Interference Shielding

- Performance and Thermal Conductivity of Polyvinylidene Fluoride-Based Lamellar Film with MXene and Graphene. *Compos. Part A: Appl. Sci. Manuf.* **2022**, 157, 106945.
23. Cho, Y.; Kim, J. Enhanced Thermal and Mechanical Properties of 3D-Printed PEG Containing Acrylate Composite with Surface-Treated BN via Digital Light Processing. *Polym. Test.* **2023**, 118, 107898.
 24. Cho, Y.; Kim, J. Effects of Two Silane Surface Modifications with Different Functional Groups on the Thermal Conductivity and Mechanical Properties of UV-Cured Composites with High Ceramic Filler Loading. *Ceram. Int.* **2022**, 48, 32001-32008.
 25. Yu, H.; Guo, P.; Qin, M.; Han, G.; Chen, L.; Feng, Y.; Feng, W. Highly Thermally Conductive Polymer Composite Enhanced by Two-Level Adjustable Boron Nitride Network with Leaf Venation Structure. *Compos. Sci. Technol.* **2022**, 222, 109406.
 26. Jang, W.; Lee, S.; Kim, N. R.; Koo, H.; Yu, J.; Yang, C. M. Eco-Friendly and Scalable Strategy to Design Electrically Insulating Boron Nitride/Polymer Composites with High through-Plane Thermal Conductivity. *Composite Part B.* **2023**, 248, 110355.
 27. An, L.; Yu, Y.; Cai, Q.; Mateti, S.; Li, L. H.; Chen, Y. I. Hexagonal Boron Nitride Nanosheets: Preparation, Heat Transport Property and Application as Thermally Conductive Fillers. *Progress in Materials Science.* **2023**, 138, 101154.
 28. Oh, H.; Kim, Y.; Wie, J.; Kim, K.; Kim, J. Tailoring of Si-C-N-O Ceramic-Coated Reduced Graphene Oxide by Oil/Water-Solution Process for High Thermal Conductive Epoxy Composite with Electrical Insulation. *Compos. Sci. Technol.* **2020**, 197, 108257.
 29. Yang, J.; Shen, X.; Yang, W.; Kim, J. K. Templating Strategies for 3D-Structured Thermally Conductive Composites: Recent Advances and Thermal Energy Applications. *Prog. Mater. Sci.* **2023**, 133, 101054.
 30. Ma, Q.; Wang, Z.; Liang, T.; Su, Y.; Li, J.; Yao, Y.; Zeng, X.; Pang, Y.; Han, M.; Zeng, X.; Xu, J.; Ren, L.; Sun, R. Unveiling the Role of Filler Surface Energy in Enhancing Thermal Conductivity and Mechanical Properties of Thermal Interface Materials. *Compos. Part A: Appl. Sci. Manuf.* **2022**, 157, 106904.
 31. Ouyang, Y.; Bai, L.; Tian, H.; Li, X.; Yuan, F. Recent Progress of Thermal Conductive Polymer Composites: Al₂O₃ Fillers, Properties and Applications. *Compos. Part A: Appl. Sci. Manuf.* **2022**, 152, 106685.
 32. Peng, X.; Qin, J.; Huang, D.; Zeng, Z.; Tang, C. Enhancement on Thermal and Mechanical Properties of Insulating Paper Cellulose Modified by Silane Coupling Agent Grafted HBN. *Macromol. Mater. Eng.* **2022**, 307, 2200424.
 33. Ozen, M.; Demircan, G.; Kisa, M.; Acikgoz, A.; Ceyhan, G.; İşiker, Y. Thermal Properties of Surface-Modified Nano-Al₂O₃/Kevlar Fiber/Epoxy Composites. *Mater. Chem. Phys.* **2022**, 278, 125689.
 34. Yang, D.; Wei, Q.; Yu, L.; Ni, Y.; Zhang, L. Natural Rubber Composites with Enhanced Thermal Conductivity Fabricated via Modification of Boron Nitride by Covalent and Non-Covalent Interactions. *Compos. Sci. Technol.* **2021**, 202, 108590.
 35. Casanova, S.; Liu, T. Y.; Chew, Y. M. J.; Livingston, A.; Mattia, D. High Flux Thin-Film Nanocomposites with Embedded Boron Nitride Nanotubes for Nanofiltration. *J. Memb. Sci.* **2020**, 597, 117749.
 36. Chen, Q.; Hao, D.; Wei, J.; Jia, C.; Wang, H.; Shi, L.; Liu, S.; Ning, F.; An, M.; Jia, Z.; Dong, F.; Ji, Y. The Influence of High-Fluorine Groundwater on Surface Soil Fluorine Levels and Their FTIR Characteristics. *Arabian J. Geosciences* **2020**, 13, 383.
 37. Khan, M. U. A.; Haider, S.; Raza, M. A.; Shah, S. A.; Razak, S. I. A.; Kadir, M. R. A.; Subhan, F.; Haider, A. Smart and PH-Sensitive RGO/Arabinosylan/Chitosan Composite for Wound Dressing: In-Vitro Drug Delivery, Antibacterial Activity, and Biological Activities. *Int. J. Biol. Macromol.* **2021**, 192, 820-831.
 38. Manu, M.; Reby Roy, K. E.; Mubarak Ali, M.; Mathew, A. A. Experimental Study on Silane as an Epoxy Additive for Improving the Impact Strength of CFRP Composites at Cryogenic Temperatures. *Mater. Today Proc.* **2021**, 52, 2279-2284.
 39. Dhali, K.; Daver, F.; Cass, P.; Adhikari, B. Surface Modification of the Cellulose Nanocrystals through Vinyl Silane Grafting. *Int. J. Biol. Macromol.* **2022**, 200, 397-408.
 40. Farrokhzad, M. A. High Temperature Oxidation Behaviour of Autocatalytic Ni-P-BN(h) Coatings. *Surf. Coat. Technol.* **2017**, 309, 390-400.
 41. Xu, W.; Yang, C.; Su, W.; Zhong, N.; Xia, X. Effective Corrosion Protection by PDA-BN@CeO₂ Nanocomposite Epoxy Coatings. *Colloids Surf A Physicochem Eng. Asp.* **2023**, 657, 130448.
 42. Mahari, S.; Gandhi, S. Electrochemical Immunosensor for Detection of Avian Salmonellosis Based on Electroactive Reduced Graphene Oxide (RGO) Modified Electrode. *Bioelectrochemistry* **2022**, 144, 108036.
 43. Sahoo, B. P.; Das, D.; Rath, P.; Chakrabarty, S.; Roy, S.; Mohanta, K. Improving Reinforcement Properties of CNTs in Aluminium Matrix Composites: A Case of Surface Modification through AlN Nano-Particle Grafting. *Surf. Interfaces* **2023**, 36, 102571.
 44. Wang, Z. Y.; Sun, X.; Wang, Y.; Liu, J. D.; Zhang, C.; Zhao, Z. B.; Du, X. Y. A High-Performance Thermally Conductive and Electrically Insulating Silver@siloxane/Graphene/Epoxy Composites at Low Filler Content: Fabrication, Mechanism Study of Insulation and Thermal Conductivity Enhancement. *Ceram. Int.* **2023**, 49, 2871-2880.

Publisher's Note The Polymer Society of Korea remains neutral with regard to jurisdictional claims in published articles and institutional affiliations.